

Image Similarity using An Ensemble of Context-Sensitive Models

Zukang Liao
University of Oxford
zukang.liao@eng.ox.ac.uk

Min Chen
University of Oxford
min.chen@oerc.ox.ac.uk

Abstract

Image similarity has been extensively studied in computer vision. In recently years, machine-learned models have shown their ability to encode more semantics than traditional multivariate metrics. However, in labelling similarity, assigning a numerical score to a pair of images is less intuitive than determining if an image A is closer to a reference image R than another image B . In this work, we present a novel approach for building an image similarity model based on labelled data in the form of $A:R$ vs $B:R$. We address the challenges of sparse sampling in the image space (R, A, B) and biases in the models trained with context-based data by using an ensemble model. In particular, we employed two ML techniques to construct such an ensemble model, namely dimensionality reduction and MLP regressors. Our testing results show that the ensemble model constructed performs $\sim 5\%$ better than the best individual context-sensitive models. They also performed better than the model trained with mixed imagery data as well as existing similarity models, e.g., CLIP [30] and DINO [3]. This work demonstrate that context-based labelling and model training can be effective when an appropriate ensemble approach is used to alleviate the limitation due to sparse sampling.

1. Introduction

Similarity between images, which has been studied for decades, is crucial for content-based retrieval [20] and image recognition [31]. In recent years, deep features have become available in metrics or models for estimating image similarity, especially those machine-learned (ML) models, e.g., through metric learning [16] or contrastive self-supervised learning [15]. While similarity scores are typically of numerical values (e.g., 0.45), there is no easy way to obtain such values as ground truth data for training or testing. In some cases, coarse-grained approximation was used to in ML processes. For example, in the dataset ROxford5k [25], labelled image pairs are grouped into four levels of similarity.

Humans' perception of image similarity is often context-sensitive (CS). In some labelling processes, binary scores were assigned to image pairs in relation to a reference image (i.e., a context), i.e., is A more similar to R than B . Such labelling processes have been shown to be more consistent and objective, and have been used in image retrieval [36], face recognition [29], and evaluation of synthesized images [38]. In these fields, the existing databases are typically used to train models that can identify closely-related images, i.e., either images (R, A) or (R, B) are very similar. For the general problem of image similarity, A and B can both be unrelated to R , as exemplified in Figure 1. Ideally, one might wish to have a vast number of image triples (R, A, B) randomly selected from an image domain \mathbb{D} . However, it would be costly to label these triples.

In this work, we considered an alternative approach, with which we selected only a small set of K reference images and the labelling effort ensured adequate sampling of (A, B) in the context of each selected reference image R_i , $i = 1..K$, as illustrated on the left of Figure 1. Each R_i group of labelled triples is refereed to as a context-sensitive (CS) data cluster. We then trained K context-sensitive (CS) models and used them to build an ensemble model. In order to answer the research questions posed in Figure 1, we compared ensemble models created using different ensemble methods as well as a model trained with a dataset where all labelled triples (R, A, B) are amalgamated. In particular, we employed two ML techniques, PCA and MLP regressors, to inform the construction of an ensemble model. Our testing showed that the resultant ensemble model performed better than the individual CS models, the model trained with mixed CS data clusters, the elementary ensemble models, and the existing similarity models, e.g., CLIP [30] and DINO [3]. This demonstrates that it is feasible to use CS data to develop models with little or very low context sensitivity, providing an efficient and effective approach for sampling image triples in the vast data space \mathbb{D}^3 .

Contributions. In summary, (1) we introduce a dataset of image similarity with 30k labelled triples, including CS data clusters and randomly-sampled triples, (2) we provide a novel method for constructing an ensemble model using

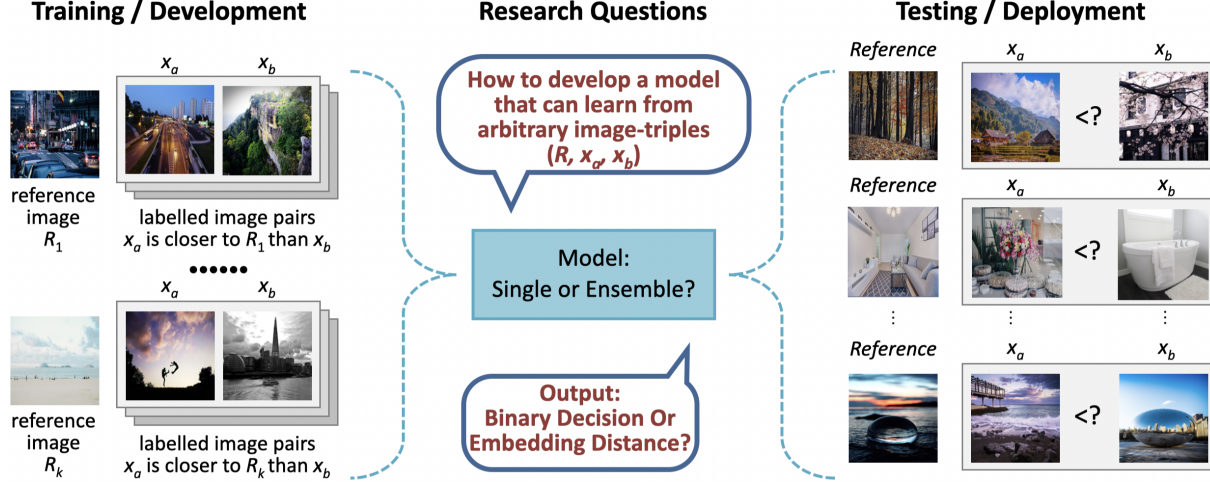


Figure 1. Given a training set of random triples that are annotated which candidate is semantically closer to the reference, can a model learn from the training data and predict correctly for unseen triples (i.e., unseen reference images and unseen candidates).

a combination of ML techniques. (3) we conduct extensive experiments to compare this approach with existing methods and some more conventional solutions, and we show that the proposed method is efficient and effective when data sampling is sparse and labelling resource is limited.

2. Related Work

In the literature, prevalent feature extractors, such as histogram of gradient/color or local binary pattern mainly focus on visual attributes of images with semantic information often being overlooked. For this reason, Wang et al.[33] introduced SDML that utilized geometric mean with normalized divergences, therefore it was able to balance inter-class divergence. The SDML distance metric was proven effective on various image classification and face recognition tasks. [11] used a combination of different distance measures, e.g., wordNet [21], Google similarity [4], and tested their method on multiple 520 random pairs collected from Flickr. Similarly, Deselaers et al. [6] studies the relationship between visual and semantic similarity on ImageNet and they introduced a new distance metric which was shown effective on image classification tasks. Zhang et al.[37] introduced a differential earth mover’s distance (DeepEMD) and their method was proven effective on various image classification tasks under k-shot setting. However, unlike context-based similarity, traditional scores are not consistent among different metrics and do not always have physical explanations. Therefore, it is necessary to revisit context-based similarity problem and provide a relatively larger dataset.

The BAPPS dataset[38] consists of 26.9k triples of reference and two distorted candidates (64x64 patches). They

provide the two alternative forced choice (2AFC) similarity annotations for the triples. Similarly, DreamSim[12] provided 20k triples of reference and two synthesized candidates (images). D’Innocente et al.[7] provided 10,805 triples of women’s dresses images. And Yoon et al.[36] ordered 1,752 triples of random images and defined a metric to evaluate the performance of image retrieval models. However, all the existing triples are carefully selected or synthesized. Therefore, at least one of the two candidates is fundamentally similar to or almost the same as the reference image. In this work, we extend the study of image similarity to arbitrarily sampled candidates.

For image similarity, the data space is gigantic. Therefore, Wray et al.[35] used proxies to largely reduce the labour cost of annotation. Similarly, Movshovitz-Attias et al. [22] used static and dynamic proxies to improve models’ performance on image retrieval and clustering tasks. Given an anchor image and a smaller subset of data points (candidates), they defined the proxy as the one with minimum distance to the anchor image. This way, they showed that the loss over proxies is a tight upper bound of the original one. Aziere et al.[1] trained an ensemble of CNNs using hard proxies to compute manifold similarity between images and their method was proven effective for image retrieval tasks. Similarly, Sanakoyeu et al.[28] introduced a divide and conquer training strategy which divided the embedding space into multiple sub-spaces and then assigned each training data object a learner according to which sub-space the training data object was located.

3. Methodology

As discussed in Section 1, the data space of image triples (R, A, B) is huge. Since human intelligence is typically

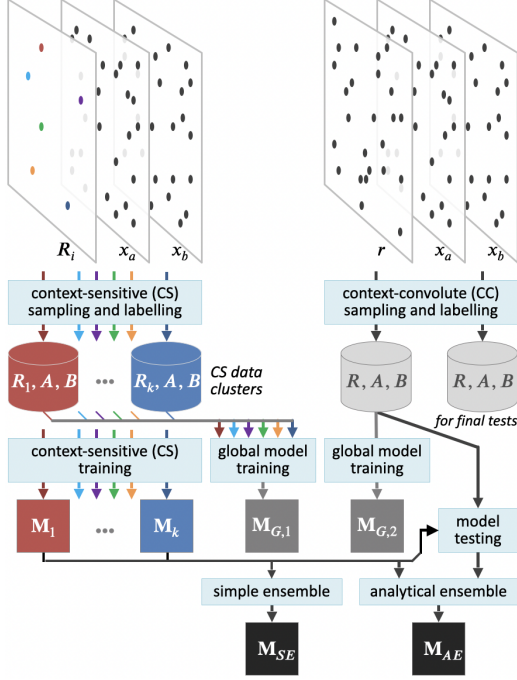


Figure 2. Overview workflow: each CS-model is trained on each CS data cluster. Analytical ensemble model is obtained based on the performance of each CS-model on the validation set. We also train global models using amalgamated data from the validation set and CS clusters for comparisons.

developed in a context-sensitive manner (e.g., most people grew up in one small region), we explore a methodology of developing similarity models based on context-sensitive (CS) learning. As illustrated in Figure 2, we selected several representative reference images, $R_i, i = 1..K$, and for each R_i , we labelled N_i image pairs (A, B) in relation to R_i . This forms K CS data clusters for training K CS models. Meanwhile, we also labelled M image triples with randomly selected reference images, and created a context-convolute (CC) dataset. The CC dataset is further divided into two subsets, one for aiding the construction of an ensemble model from the K CS models, and the other for evaluating all models in an unbiased manner. In the following subsections, we detail the training of CS models and the construction of ensemble models.

3.1. Training Context-Sensitive (CS) Models

As shown in Figure 2, we trained K CS models M_i , each based on a CS data cluster. For the purpose of comparative evaluation, we used the same approach to train two global models, $M_{G,1}$ and $M_{G,2}$. The former is trained with a mixture of CS data, while the latter with CC data.

Training Paradigm. As shown in Figure 3, we use a standard training procedure with both triplet loss and cross entropy loss for the ranking block (binary classifier). The

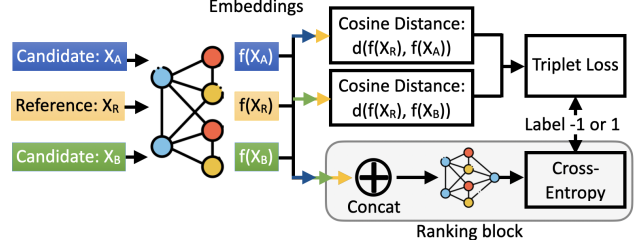


Figure 3. To train each CS model, we concatenate the embeddings, and train a small ranking block to conduct binary classification. The cross entropy loss of the ranking block, triplet loss, and LoRA [14] are used to assist fine-tuning the backbone.

ranking block is helpful when the data is sparse or when the backbone is not a large model, e.g., resnet18. When the backbone is large, e.g., ViT, Lora [14] is used to reduce the number of trainable weights. We show simply using the cross entropy loss alone can achieve satisfactory accuracy for each CS model in the ablation study in the Appendix A.

Context-based Triplet Loss. The (R, A, B) triples that we used in the work are conceptually similar to the traditional contrastive / triplet loss setting (anchor, positive, negative) in deep metric learning. However, instead of pulling positive examples closer to the anchor whilst pushing negative examples away from the anchor, the selection of the two candidates A and B is random. One can switch A and B or flip the annotation for similarity augmentation. Therefore, it is not always appropriate to push A or pull B . Formally, we define the triplet loss function as:

$$L_{\text{diff}} := (d(f(x_r), f(x_a)) - d(f(x_{\text{ref}}), f(x_b))) \times y$$

$$L_{\text{triplet}} := \max(\text{margin} - L_{\text{diff}}, 0)$$

where f represents the backbone of an ML model (M), $f(x)$ denotes the embedding of an input x to M , d is a traditional distance function between two embeddings (e.g., cosine distance), and y is the annotated similarity label of the triple (x_r, x_a, x_b) that also controls the sign of the loss function. For example, when $y = -1$ (x_r is closer to candidate x_a), minimizing the loss function will reduce the distance between the reference and the closer candidate (x_a) whilst increasing the distance between the reference and the other candidate (x_b). We set the margin to 0.1. Note that, unlike image retrieval or ReID, the triplet loss is not naturally zero everywhere due to the randomised selection of the two candidates. Therefore, we did not use any mining strategy for the triplet loss.

3.2. Ensemble Strategies

As shown in Figure 2, we used simple ensemble strategy, voting, to create a baseline benchmark for more complex ensemble strategies.

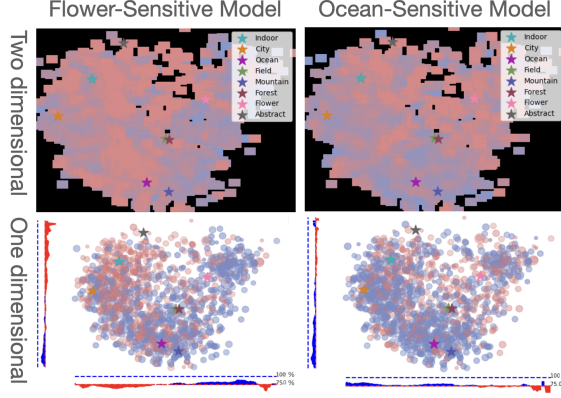


Figure 4. Ensemble Approach (PCA): We extract features of reference images using a neural net, e.g., ViT, and visualize them using PCA or tSNE. We then compute the accuracy (represented by colors) for every single reference image using each CS model. An ensemble method can be obtained based on the scatter plots.

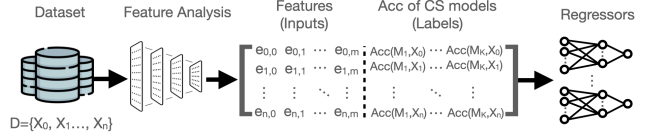
Context-Convolute (CC) Testing. While one may train a set of CS models, one would like to use these models to construct an ensemble that can be applied other contexts. We thus used CC data to test CS models as shown in Figure 2 (bottom-right). This particular subset of CC data is referred to as a validation dataset \mathbb{T}_V . For each image triple $(x_r, x_a, x_b) \in \mathbb{T}_V$ and each CS model $M_i, i = 1..K$, the testing yields a correctness indicator. The total number of such indicators is $|\mathbb{T}_V| \times K$. The testing can also result in additional information, such as confusion matrix and uncertainty or confidence values. The CC testing results can inform the construction of ensemble models.

Feature-based Analysis and Specialization. Given a large set of images, one can extract l features, which define an l -D feature space of the images. These features can be the results of dimensionality reduction techniques such as PCA and t-SNE as well as hand-crafted feature extraction algorithms. Each image can thus be encoded as an l -D feature vector $\Theta = [\theta_1, \theta_2, \dots, \theta_l]$.

For an arbitrary reference image x_r , its feature vector Θ_r determines its l -D coordinates in the feature space. When a triple (x_r, x_a, x_b) is tested against a CS model M_i , the correctness indicator can be considered as a sample of a correctness manifold at position Θ . With K CS models, we have K such manifolds based on correctness indicators. The testing of a CS model M_i with the validation set, gave us a way to establish an approximate model of the manifold that can be used to predict the correctness of applying M_i to a previously-unseen image triple.

Ensemble based on Credibility Maps. An l -D *credibility map* of a model M_i is a discrete partition of the l -D feature space into a number of l -D cells, and each cell stores a value (or values) indicating the probability of M_i to be correct when it applies to image triples whose feature vectors

Development / Training



Deployment / Testing

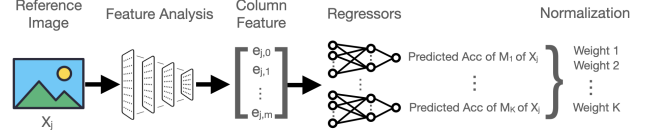


Figure 5. Ensemble Approach (MLP): MLP regressors are trained to predict the performance of each CS model using features extracted from a dataset of reference images. Given a reference image, the predicted accuracy scores of each CS model can be used as the tailored ensemble weights for the reference image.

that fall into the cell. Figure 4 illustrates such credibility maps in 1D and 2D sub-spaces. The two plots above show the 2D credibility maps of two CS models trained using the flower data cluster and ocean data cluster respectively. Each of the 2D manifolds is sampled with 12k triples in \mathbb{T}_V , and the 2D feature subspace is partitioned into 200^2 cells. The two images below include four line plots representing four 1D credibility maps. Each line plot results from the projection of a set of testing results. From Figure 4, we can observe that these credibility maps can provide useful information about the past and potential performance of different CS models in different parts of the feature space.

One ensemble strategy is to determine, for each image triple (x_r, x_a, x_b) , how much each CS model should contribute to the decision. The feature vector of (x_r, x_a, x_b) can be used to look-up relevant cells in one of more credibility maps. Likely partitioning a high dimensional feature space will result in many empty cells. A practical solution is for an ensemble algorithm to consult several low dimensional credibility maps for each CS model, and aggregate the credibility values into a single credibility score per CS model. The scores for different CS models can then be used to determine the contribution of each CS Model in the final decision specifically for image triple (x_r, x_a, x_b) .

One may adopt of one of the commonly-used ensemble algorithm, e.g., (i) use these scores to filter out some CS models in the final decision process before voting, (ii) normalize these scores into a set of weights, and make a decision based on weighted votes, (iii) filter first and then compute weighted votes, and so on.

ML-Based Ensemble Strategy. The weights of the CS models can also be produced by another ML model, which is trained using the feature vectors as inputs and the testing results as correctness labels. In this work, we show that,

Table 1. Comparison with existing datasets of triples

Dataset	Input Type	Size	Annotators	Data Source	Candidate Restriction	Random Candidates
Yoon et al.[36]	Images	1,752	5.7	Visual Genome[17], MS-COCO[19]	Similar to the reference	✗
BAPPS (real-algo)[38]	64x64 Patches	26.9k	2.6	MIT-Adobe5k[2], RAISE1k[5]	Distorted from the reference	✗
NIGHTS[12]	Images	20k	7.1	Diffusion[27]-synthesized	Synthesized from the reference	✗
CoSIS (Ours)	Images	30k	3	BG20k[18]	No Restriction	✓

with a relatively small validation set (12K triples), an ML model can still learn to predict the weights of CS models. As shown in Figure 5, firstly, we extract features of the reference images in the validation set using a neural net (e.g., ViT), and we then use a dimensionality reduction method (e.g., PCA) to extract important features. Dimensionality reduction counteracts the sparseness of the testing data. In our main implementation, we used 64 dimensions. The features are then fed to several simple multi-layer perceptron (MLP) regressors, each of which is trained to predict the accuracy score of one CS model given an input reference image. In deployment process, given a reference image (input), accuracy scores of all CS models are estimated by the MLP regressors. The normalized accuracy scores are used as the weights for determining the contribution of each CS model for the specific reference image.

4. Datasets

As part of this work, we provide a new image similarity dataset (CoSIS), which currently consists of 30k labelled triples. The CoSIS dataset has 8k context-sensitive (CS) triples, which is divided into eight CS training sets (1k each) namely *Indoor*, *City*, *Ocean*, *Field*, *Mountain*, *Forest*, *Flower*, and *Abstract*. The CoSIS also contains 22k context-convolute (CC) triples, which is divided into two subsets, a validation set (12k) and a testing set (10k) for evaluating all models in an unbiased manner. As shown in Table 1, unlike existing datasets of triples in the literature, e.g., BAPPS [38], in both CS and CC portions of CoSIS, the two candidates x_a and x_b are selected randomly. Therefore, there is no guarantee that any of the candidate is semantically similar to or the same as the reference image x_r . The images of the triples are from the BG20k dataset [18], which consists of 20k background images. Hence the data space of the triples is of the size of $\|\mathbb{D}^3\| = (20k)^3$.

Two-Alternative Forced-Choice (2AFC). For each of the 30k triples (x_r, x_a, x_b) , we provide binary annotation: -1 if x_a is considered closer to x_r , and 1 otherwise.

Each triple is labelled by three annotators. Among the three annotators, our inter-rater reliability score is 0.947 which is higher than most cognitive tasks, e.g., emotion detection and many NLP tasks [9]. In some cases, we discarded triples when: (i) annotators considered two candidates x_a and x_b were very similar and equally distanced from the reference (e.g., they are both snowy mountains),

and (ii) when both x_a and x_b are totally irrelevant to the reference image x_r (e.g., a desert and an ocean are both almost completely irrelevant to a kitchen). With random selection, cases of (i) are relatively rare ($\leq 4\%$), while cases of (ii) are more common (around 14%).

Context-Sensitive (CS) Training Sets. For each representative reference image R_i , we collect 1,000 triples where the two candidates x_a and x_b are randomly selected. We denote it as a CS dataset \mathbb{T}_{CS_i} . CoSIS currently has eight CS datasets based on the eight categories defined by [10]. The eight representative reference images are: Indoor (#715), City (#2723), Ocean (#389), Field (#1673), Mountain (#1006), Forest (#254), Flower (#2352), and Abstract (#667). Note that when training and evaluating each CS model on a CS dataset D_{CS_i} , we split the 1,000 triples into 667 for training and 333 for validation.

Context-Convolute (CC) Data. These randomly selected triples were labelled for aiding the analytical ensemble strategies and evaluating fairly the performance of all models concerned. The CC data set has 22,008 triples with 2,330 unique reference images. Three images in each triple are randomly selected, and each unique reference image has at least 9 labelled triples. Therefore, the testing results for each single reference image are reasonably statistical significant. We further split the 22k random triples into a validation set (12,006 triples with 1,320 unique reference images) and a testing set (10,002 triples with 1,010 unique reference images). Note that the testing set does not overlap with either the validation set or any CS training set, in terms of both reference images and candidate images.

Data Cleaning. Among the three annotators, when there were disagreements, we used majority votes as the final labels. In the original labelled triples, there were some loops (e.g., with reference R , A is closer than B , B is closer than C , C is closer than A). We found only 0.11% triples that were in at least a loop, and the longest loop involves four candidates. These triples were removed from the dataset.

5. Experiment

We conducted extensive tests under different settings, including different model architectures, e.g., ResNet, VGG, and ViT that are pre-trained on different datasets, e.g., ImageNet, Place365, and Google Landmarks Dataset (v2) [34].

Table 2. Performance of existing supervised and self-supervised models on different context-sensitive (CS) testing datasets.

<i>Traditional Similarity Metrics and Deep Image Retrieval Models</i>									
Reference Image	#Indoor	#City	#Ocean	#Field	#Mountain	#Forest	#Flower	#Abstract	Average
HesAff SIFT+SP[23]	66.8%	60.0%	55.1%	41.8%	53.3%	37.7%	54.4%	59.2%	53.5%
GeM-ResNet50[26]	73.7%	77.6%	75.1%	71.0%	68.0%	77.2%	73.9%	55.9%	71.6%
SfM-ResNet50[24]	81.9%	81.6%	85.8%	69.5%	83.3%	74.8%	73.6%	69.8%	77.5%

<i>Large Self-Supervised Models Trained on Large Datasets</i>									
Reference Image	#Indoor	#City	#Ocean	#Field	#Mountain	#Forest	#Flower	#Abstract	Average
DINO[3]-ResNet50	69.2%	81.2%	76.6%	70.7%	81.7%	74.6%	77.8%	49.2%	72.6%
DINO[3]-ViT-B16	74.6%	83.3%	83.8%	69.0%	87.7%	72.5%	75.4%	70.3%	77.1%
CLIP[30]-ViT-B32	70.1%	78.8%	82.9%	68.7%	85.6%	79.0%	77.2%	80.8%	77.9%

<i>Embedding Distances Based on Backbones of Supervised Models Trained on Large Datasets</i>									
Reference Image	#Indoor	#City	#Ocean	#Field	#Mountain	#Forest	#Flower	#Abstract	Average
ResNet18-Place365[39]	61.1%	78.2%	78.1%	69.6%	83.8%	77.5%	72.1%	72.1%	74.1%
ResNet18-ImageNet[13]	76.9%	82.4%	81.1%	66.0%	87.4%	72.2%	66.1%	67.6%	75.0%
VGG16-ImageNet[32]	81.4%	82.7%	88.9%	62.4%	88.6%	75.4%	70.6%	67.0%	77.1%
ViT-ImageNet[8]	82.3%	83.1%	83.0%	76.0%	87.4%	83.8%	86.8%	72.9%	81.9%

Table 3. Performance of different context-sensitive CS models (trained on the CS training dataset) on the corresponding testing dataset.

<i>Our Context-Sensitive Models - Different Pre-trained Architectures</i>									
Reference Image	#Indoor	#City	#Ocean	#Field	#Mountain	#Forest	#Flower	#Abstract	Average
VGG16-ImageNet	86.2%	86.6%	86.1%	90.1%	87.8%	76.9%	72.3%	74.5%	82.6%
ResNet18-ImageNet	88.0%	86.0%	88.0%	78.8%	90.4%	82.9%	85.5%	79.3%	84.8%
ResNet18-Place365	86.5%	87.5%	88.6%	88.1%	90.4%	77.8%	70.6%	83.8%	84.2%
ViT-Lora	80.2%	82.7%	89.5%	83.6%	90.7%	86.2%	86.8%	78.4%	84.8%

5.1. Overview of Our Fine-tuned Models

CS Models. We train eight CS models $M_i, i = 1..8$, each of which is trained on one CS dataset with the training-split (667 CS triples).

Global Models. One is a single model trained on the CC validation set (12k) and another is trained on the amalgamated CS training sets (8k in total).

Ensemble Models. These made use of different CS models, and the ensemble strategies were derived from the results of testing CS models on the validation set (12k).

5.2. Performance of Context-Sensitive (CS) Models

Performance on the CS Training Sets. For each CS dataset (1k), we split the data into 667 triples for training, and 333 triples for reporting the performance of models. As shown in Table 2, using embedding distances from image retrieval models achieved around 70%~78%, and large self-supervised models, e.g., CLIP/DINO, and supervised models, e.g., ViT, were able to achieve 78%~82%. To investigate whether we can improve the performance, we fine-tuned several models of different architectures. As shown in Table 3, the fine-tuned CS models outperform all existing methods on their corresponding CS datasets. In Appendix E, we show more results on using different architectures. Due to the limited number of labelled data, compared

with ResNet18 and VGGNets, directly fine-tuning models with a larger architecture might not be effective, e.g., ResNet34 and ResNet50 reached around 60%~65% whilst ResNet18 and VGGNets reached around 81%~84% on average. Therefore, we fine-tuned larger and deeper models with LoRA[14] to boost the performance. Fine-tuning ViT with Lora (denoted as ViT-Lora) achieved the best averaged accuracy (around 85%), which is aligned with the most recent studies on evaluating synthesized images using labelled triples [12, 38].

In Table 3, we highlight the best CS model trained using each CS dataset. When assembling CS models, we do not need to always select the ones with the same architecture and we can use the eight highlighted models to form our ensemble models. These eight CS models achieved 84%~91% on the CS datasets, which is significantly better than any of the existing methods in Table 2. Such improvement is expected because the models are fine-tuned on the CS datasets whilst the existing models are not. Nevertheless, the results suggest that the CS models can perform

Table 4. Performance of CS models on random triples

Model	Indoor	City	Ocean	Field	Mountain	Forest	Flower	Abstract
Validation Set	77.3%	75.4%	78.3%	73.3%	79.5%	75.7%	76.6%	79.3%
Testing Set	76.9%	74.3%	78.4%	72.7%	79.1%	73.9%	73.9%	77.2%

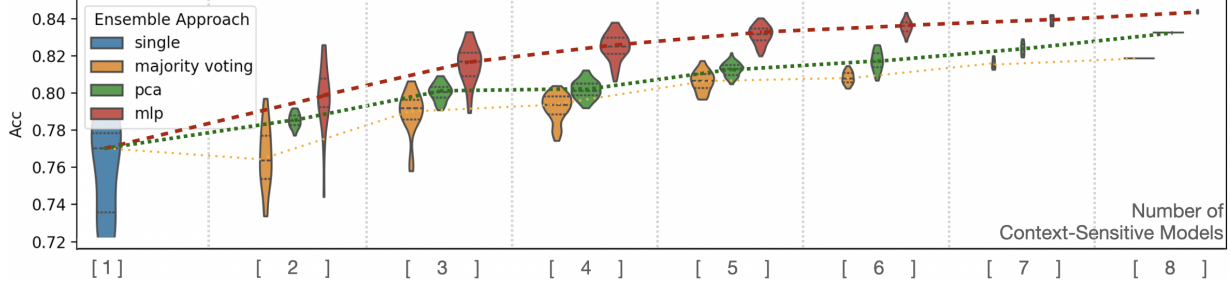


Figure 6. Y-axis: accuracy of the ensemble methods on the testing set (10k). X-axis: the number of CS models used to form the ensemble model. Experiments are run on all the combinations, e.g., when choosing two CS models, we run experiments on all of the $C_2^8 = \frac{8!}{2! \cdot 6!} = 28$ combinations. For MLP, we repeat the same experiment three times for one combination, e.g., for choosing two CS models, we run $3 \cdot C_2^8 = 84$ experiments. MLP-based approach consistently performs the best. Dashed lines inside the blobs are the quartiles of the data.

Table 5. Performance of Ensemble Models on Randomly Selected Triples. Validation Set: 12k triples. Testing Set: 10k triples.

	Existing models					Our models			
	GeM[26]	ResNet18[13]	DINO[3]	CLIP[30]	ViT[8]	Best Single	Majority Vote	Ensemble(PCA)	Ensemble(MLP)
Validation Set	73.5%	77.6%	78.5%	77.4%	80.4%	79.5%	82.3%	87.0%	86.6% \pm 0.5%
Testing Set	72.7%	77.7%	77.7%	75.7%	79.9%	79.1%	81.9%	83.3%	84.7% \pm 0.3%

Table 6. Performance of global models on the testing set (10k)

Training Set Architecture	No Training Embedding Distance	Context Training Set (8k)	Validation Set (12k)
VGG16	78.3%	71.4% \pm 4.2%	77.3% \pm 2.0%
ResNet18	77.7%	72.1% \pm 1.9%	80.2% \pm 1.6%
ViT-Lora	79.9%	68.9% \pm 3.6%	79.6% \pm 1.3%

well on unseen candidates x_a and x_b . In the appendix D, we show and discuss more experiments involving training CS models using more than one CS datasets.

Performance on the CC Validation (12k) / Testing Set (10k): To evaluate how the selected CS models perform on unseen reference images, we run each CS model M_i on the CC validation and testing set. As shown in Table 4, the CS models achieved 73%~79.5%, which is lower than the results they achieved on the CS clusters. And the results are also lower or similar to the existing models, e.g., ViT, as shown in Table 5.

5.3. Performance of Global Models

As shown in Figure 2, we trained two global models, M_{G1} and M_{G2} . The former was trained with an amalgamation of the eight CS data clusters (8k in total), and the latter was trained with the CC validation set (12k random triples). Three architectures were used. Table 6 shows the results of testing these models against the CC testing set (10k).

The global models trained on the CC validation set achieved 77%~80% on average, which is similar to existing models, e.g., ViT: ~80% and ResNet18: ~77%, which are not trained on any of our labelled data. Additionally, training on all of our context training set (8k) does not improve the performance on the testing set either. Moreover, training

one single model on all of the amalgamated context datasets led to a decrease in accuracy on the testing set (69%~72%) compared with their untrained counterparts (77%~80%). This might be caused by the sparsity of the context training set which only contains eight reference images.

5.4. Performance of Ensemble Models

Experiments on the Validation Set (12k). Based on each CS model’s performance (e.g., visualized in Figure 4) on the validation set, we obtain the weights of the ensemble model(s) using two methods: PCA, and MLP as specified in Section 3. As shown in Table 5, our ensemble models perform 8%~10% higher than all existing models, the best CS model, the global model and simple ensemble approach (majority voting) on the validation set. The improvement is expected as the ensemble weights are obtained directly from the validation set.

Experiments on the Testing Set (10k). To show the ability of our ensemble models on unseen reference and candidate images, we run the models on the testing set which has no overlapping with the validation set or the context training set. Table 5 shows that our ensemble approaches perform ~5% better than existing models, the best CS model, the global model and majority voting. The results show that our ensemble model can also perform relatively well on unseen reference images and candidate images.

5.5. Result Analysis and Training Visualization

Number of Context-Sensitive Models Figure 6 shows the accuracy on the testing set of the three ensemble approaches (Majority Voting, PCA, and MLP) when using different numbers of CS models to form the ensemble models. For

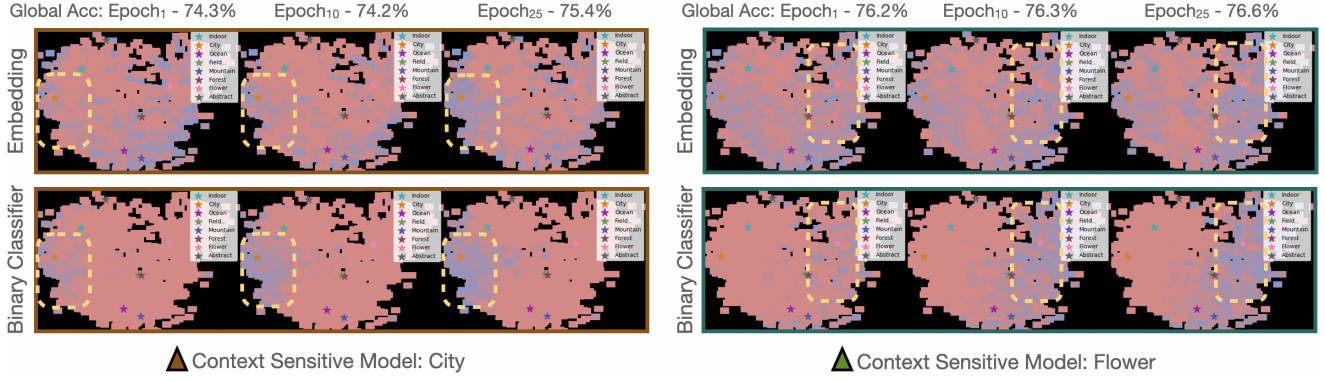


Figure 7. Visualized CS training: the local performance (highlighted areas) is improved gradually during training, whilst the global accuracy remains stable. The second row shows the changes of binary classifiers’ performance from scratch. It is more noticeable that the performance on the highlighted areas are constantly improving during training. The first row shows that we can also see the same improvement on the highlighted areas when using embeddings, especially when comparing the results in the beginning and end of CS training. This shows that CS training improves local performance for both binary classifier and using embeddings. The bluer, the more accurate of the CS model that is being trained, whilst red indicates accuracy $\leq 75\%$.

a number of selected CS models, we run experiments on all possible combinations. To be specific, when selecting r from the $n = 8$ CS models where $r = \{1, 2, \dots, n\}$, we run experiments on all of the $C_r^n = \frac{n!}{(n-r)! \cdot r!}$ combinations. For the MLP-based ensemble approach, we repeat the same experiments three times for one given combination, which leads to $3 * C_r^n$ runs of experiments for the MLP-based ensemble approach. The results show that MLP-based approach consistently performs the best, and both of our proposed approaches (MLP-based and PCA-based) perform constantly better than simple ensemble method, e.g., majority voting. In addition, the results indicate that the accuracy scores on the testing set starts to saturate when we use more than six CS models. This might be the reason that the field-sensitive model, forest-sensitive model and mountain-sensitive model learn similar rules and perform similarly on the testing set. Therefore, assembling these similar CS models might not lead to a significant increase in global accuracy on the testing set. In Appendix B, we conduct cross validation of the CS models on the CS clusters, and in Appendix C, we study the impact of each CS model on the ensemble models by showing their shapley values.

Visualization of CS Training Process: We visualize the CS training process by showing testing results (on the validation set) at the end of each training epoch, as well as reporting a global accuracy score (on the validation set) for each epoch. As shown in Figure 7, as the CS models are being trained, the global accuracy almost remains unchanged, i.e., $\sim 74.5\%$ and $\sim 76\%$ for the city- and flower-sensitive model. Note that the binary classifiers are trained from scratch, and therefore it is noticeable that the performance improves gradually during training for some specific

area (the second row). We highlight the area where we see the improvement from the binary classifiers, and we show that we can also see the improvement when using embeddings within the highlighted area (the first row). This shows that CS training is able to improve local performance, and more visualized training processes of other CS models can be found in Appendix E.

6. Conclusions

In this paper, we addressed a new problem of developing image similarity models based on context-sensitive (CS) training datasets that contain images triples (R, A, B) focusing only on a few reference images. We trained a set of CS models, and our tests showed their ability to improve performance locally in their corresponding contexts but not globally when being applied to other contexts. We introduced a new approach to estimate a correctness manifold for each CS model based on imagery features and the testing results of the CS model. The estimated manifolds of CS models enable an ensemble strategy that predicts the correctness probability of each CS model dynamically for each input triple (R, A, B) and determines the contribution of CS models accordingly. Our extensive experiments showed that our proposed methods performed the best in comparison with all existing models, simple ensemble models, and trained CS and global models.

In addition, we have collected a dataset of 30k labelled triples, including eight CS training data sets (1k each) and a context-convolute (CC) dataset (22k). We are in the process of making this CoSIS dataset available in the public domain.

In future work, we will further explore the paradigm of constructing ensemble models using CS models, which in many ways bears some similarity to human learning.

References

- [1] Nicolas Aziere and Sinisa Todorovic. Ensemble deep manifold similarity learning using hard proxies. In *Proceedings of the IEEE/CVF Conference on Computer Vision and Pattern Recognition*, pages 7299–7307, 2019. 2, 14
- [2] Vladimir Bychkovsky, Sylvain Paris, Eric Chan, and Frédo Durand. Learning photographic global tonal adjustment with a database of input / output image pairs. In *The Twenty-Fourth IEEE Conference on Computer Vision and Pattern Recognition*, 2011. 5
- [3] Mathilde Caron, Hugo Touvron, Ishan Misra, Hervé Jégou, Julien Mairal, Piotr Bojanowski, and Armand Joulin. Emerging properties in self-supervised vision transformers. In *Proceedings of the International Conference on Computer Vision (ICCV)*, 2021. 1, 6, 7
- [4] Rudi L Cilibrasi and Paul MB Vitanyi. The google similarity distance. *IEEE Transactions on knowledge and data engineering*, 19(3):370–383, 2007. 2
- [5] Duc-Tien Dang-Nguyen, Cecilia Pasquini, Valentina Conotter, and Giulia Boato. Raise: A raw images dataset for digital image forensics. In *Proceedings of the 6th ACM multimedia systems conference*, pages 219–224, 2015. 5
- [6] Thomas Deselaers and Vittorio Ferrari. Visual and semantic similarity in imagenet. In *CVPR 2011*, pages 1777–1784. IEEE, 2011. 2
- [7] Antonio D’Innocente, Nikhil Garg, Yuan Zhang, Loris Baz-zani, and Michael Donoser. Localized triplet loss for fine-grained fashion image retrieval. In *Proceedings of the IEEE/CVF conference on computer vision and pattern recognition*, pages 3910–3915, 2021. 2
- [8] Alexey Dosovitskiy, Lucas Beyer, Alexander Kolesnikov, Dirk Weissenborn, Xiaohua Zhai, Thomas Unterthiner, Mostafa Dehghani, Matthias Minderer, Georg Heigold, Sylvain Gelly, et al. An image is worth 16x16 words: Transformers for image recognition at scale. *arXiv preprint arXiv:2010.11929*, 1, 2020. 6, 7
- [9] N El Dehaibi and EF MacDonald. Investigating inter-rater reliability of qualitative text annotations in machine learning datasets. In *Proceedings of the Design Society: DESIGN Conference*, pages 21–30. Cambridge University Press, 2020. 5
- [10] Hui Fang, Gary Kwok-Leung Tam, Rita Borgo, Andrew J Aubrey, Philip W Grant, Paul L Rosin, Christian Wallraven, Douglas Cunningham, David Marshall, and Min Chen. Visualizing natural image statistics. *IEEE Transactions on Visualization and Computer Graphics*, 19(7):1228–1241, 2012. 5
- [11] Valentina Franzoni, Alfredo Milani, Simonetta Pallottelli, Clement HC Leung, and Yuanxi Li. Context-based image semantic similarity. In *2015 12th international conference on fuzzy systems and knowledge discovery (fskd)*, pages 1280–1284. IEEE, 2015. 2
- [12] Stephanie Fu, Netanel Tamir, Shobhita Sundaram, Lucy Chai, Richard Zhang, Tali Dekel, and Phillip Isola. Dream-sim: Learning new dimensions of human visual similarity using synthetic data. *arXiv preprint arXiv:2306.09344*, 2023. 2, 5, 6
- [13] Kaiming He, Xiangyu Zhang, Shaoqing Ren, and Jian Sun. Deep residual learning for image recognition. In *Proceedings of the IEEE conference on computer vision and pattern recognition*, pages 770–778, 2016. 6, 7
- [14] Edward J Hu, Yelong Shen, Phillip Wallis, Zeyuan Allen-Zhu, Yuanzhi Li, Shean Wang, Lu Wang, and Weizhu Chen. Lora: Low-rank adaptation of large language models. *arXiv preprint arXiv:2106.09685*, 2021. 3, 6, 15
- [15] Ashish Jaiswal, Ashwin Ramesh Babu, Mohammad Zaki Zadeh, Debapriya Banerjee, and Fillia Makedon. A survey on contrastive self-supervised learning. *Technologies*, 9(1): 2, 2020. 1
- [16] Mahmut Kaya and Hasan Şakir Bilge. Deep metric learning: A survey. *Symmetry*, 11(9):1066, 2019. 1
- [17] Ranjay Krishna, Yuke Zhu, Oliver Groth, Justin Johnson, Kenji Hata, Joshua Kravitz, Stephanie Chen, Yannis Kalantidis, Li-Jia Li, David A Shamma, et al. Visual genome: Connecting language and vision using crowdsourced dense image annotations. *International journal of computer vision*, 123:32–73, 2017. 5
- [18] Jizhi Li, Jing Zhang, Stephen J Maybank, and Dacheng Tao. Bridging composite and real: towards end-to-end deep image matting. *International Journal of Computer Vision*, 130:246–266, 2022. 5
- [19] Tsung-Yi Lin, Michael Maire, Serge Belongie, James Hays, Pietro Perona, Deva Ramanan, Piotr Dollár, and C Lawrence Zitnick. Microsoft coco: Common objects in context. In *Computer Vision—ECCV 2014: 13th European Conference, Zurich, Switzerland, September 6–12, 2014, Proceedings, Part V 13*, pages 740–755. Springer, 2014. 5
- [20] Jiayi Ma, Xingyu Jiang, Aoxiang Fan, Junjun Jiang, and Junchi Yan. Image matching from handcrafted to deep features: A survey. *International Journal of Computer Vision*, 129:23–79, 2021. 1
- [21] George A Miller. Wordnet: a lexical database for english. *Communications of the ACM*, 38(11):39–41, 1995. 2
- [22] Yair Movshovitz-Attias, Alexander Toshev, Thomas K Leung, Sergey Ioffe, and Saurabh Singh. No fuss distance metric learning using proxies. In *Proceedings of the IEEE international conference on computer vision*, pages 360–368, 2017. 2
- [23] Michal Perd’och, Ondrej Chum, and Jiri Matas. Efficient representation of local geometry for large scale object retrieval. In *2009 IEEE Conference on Computer Vision and Pattern Recognition*, pages 9–16. IEEE, 2009. 6
- [24] F. Radenović, G. Tolias, and O. Chum. CNN image retrieval learns from BoW: Unsupervised fine-tuning with hard examples. In *ECCV*, 2016. 6
- [25] Filip Radenović, Ahmet Iscen, Giorgos Tolias, Yannis Avrithis, and Ondřej Chum. Revisiting oxford and paris: Large-scale image retrieval benchmarking. In *Proceedings of the IEEE conference on computer vision and pattern recognition*, pages 5706–5715, 2018. 1
- [26] F. Radenović, G. Tolias, and O. Chum. Fine-tuning CNN image retrieval with no human annotation. *TPAMI*, 2018. 6, 7
- [27] Robin Rombach, Andreas Blattmann, Dominik Lorenz, Patrick Esser, and Björn Ommer. High-resolution image

- synthesis with latent diffusion models. In *Proceedings of the IEEE/CVF conference on computer vision and pattern recognition*, pages 10684–10695, 2022. 5
- [28] Artsiom Sanakoyeu, Vadim Tschernezki, Uta Buchler, and Bjorn Ommer. Divide and conquer the embedding space for metric learning. In *Proceedings of the IEEE/CVF conference on computer vision and pattern recognition*, pages 471–480, 2019. 2
- [29] Florian Schroff, Dmitry Kalenichenko, and James Philbin. Facenet: A unified embedding for face recognition and clustering. In *Proceedings of the IEEE conference on computer vision and pattern recognition*, pages 815–823, 2015. 1
- [30] Christoph Schuhmann, Romain Beaumont, Richard Vencu, Cade W Gordon, Ross Wightman, Mehdi Cherti, Theo Coombes, Aarush Katta, Clayton Mullis, Mitchell Wortsman, Patrick Schramowski, Srivatsa R Kundurthy, Katherine Crowson, Ludwig Schmidt, Robert Kaczmarczyk, and Jenia Jitsev. LAION-5b: An open large-scale dataset for training next generation image-text models. In *Thirty-sixth Conference on Neural Information Processing Systems Datasets and Benchmarks Track*, 2022. 1, 6, 7
- [31] Muhammad Shafiq and Zhaoquan Gu. Deep residual learning for image recognition: A survey. *Applied Sciences*, 12(18):8972, 2022. 1
- [32] Karen Simonyan and Andrew Zisserman. Very deep convolutional networks for large-scale image recognition. *arXiv preprint arXiv:1409.1556*, 2014. 6
- [33] Huibing Wang, Lin Feng, Jing Zhang, and Yang Liu. Semantic discriminative metric learning for image similarity measurement. *IEEE Transactions on Multimedia*, 18(8):1579–1589, 2016. 2
- [34] Tobias Weyand, Andre Araujo, Bingyi Cao, and Jack Sim. Google landmarks dataset v2-a large-scale benchmark for instance-level recognition and retrieval. In *Proceedings of the IEEE/CVF conference on computer vision and pattern recognition*, pages 2575–2584, 2020. 5
- [35] Michael Wray, Hazel Doughty, and Dima Damen. On semantic similarity in video retrieval. In *Proceedings of the IEEE/CVF Conference on Computer Vision and Pattern Recognition*, pages 3650–3660, 2021. 2
- [36] Sangwoong Yoon, Woo Young Kang, Sungwook Jeon, SeongEun Lee, Changjin Han, Jonghun Park, and Eun-Sol Kim. Image-to-image retrieval by learning similarity between scene graphs. In *Proceedings of the AAAI Conference on Artificial Intelligence*, pages 10718–10726, 2021. 1, 2, 5
- [37] Chi Zhang, Yujun Cai, Guosheng Lin, and Chunhua Shen. Deepemd: Few-shot image classification with differentiable earth mover’s distance and structured classifiers. In *Proceedings of the IEEE/CVF conference on computer vision and pattern recognition*, pages 12203–12213, 2020. 2
- [38] Richard Zhang, Phillip Isola, Alexei A Efros, Eli Shechtman, and Oliver Wang. The unreasonable effectiveness of deep features as a perceptual metric. In *Proceedings of the IEEE conference on computer vision and pattern recognition*, pages 586–595, 2018. 1, 2, 5, 6
- [39] Bolei Zhou, Agata Lapedriza, Aditya Khosla, Aude Oliva, and Antonio Torralba. Places: A 10 million image database for scene recognition. *IEEE transactions on pattern analysis and machine intelligence*, 40:1452–1464, 2017. 6

Appendices A ~ E

In **Appendix A**, we present a set of experiments in addition to those were reported in Section 5.2, including results that complement the results in Table 4. In particular, the results indicated that the models using embeddings to compute the cosine distance between two images are more suitable for building ensemble models than binary classifiers.

In **Appendix B**, we present a set of early experiments where each CS model (using embedding distance) is applied on different CS clusters. The results indicate that some CS models can perform reasonably on data belong to other CS clusters, while some others performed poorly. This suggests that (i) CS models can potentially be applied to context-convolute (CC) data, and (ii) the suitability can be inferred from testing results. The experiments provides an early hypothesis that motivated the work outlined in the paper.

In **Appendix C**, we present a set of further experiments, where We intentionally exclude each CS model from an ensemble, and test such an ensemble (i.e., missing X CS model) against different CS datasets (including the X CS dataset). The results show that such an ensemble model can perform fairly well, indicating that it possesses a fair amount of knowledge about the missing X CS model. This set of experiments further support the suggestions that (i) CS models can potentially be applied to context-convolute (CC) data, and (ii) the suitability can be inferred from testing results.

In **Appendix D**, we present several experiments for testing the hypothesis that combining some CS training datasets might improve the CS model concerned. Our experiments indicate that simply combining the CS training datasets that we have cannot improve the performance. This suggests broadening the context by combining k CS training datasets may require much more data than simply adding the k datasets together. It also leads to a decision to focus on ensemble models constructed using the CS models that are trained on only one CS data cluster.

In **Appendix E**, we show additional experimental results (with different architectures) to complement Table 3 in Section 5.2 and we also show additional visualization results (for different CS models) to complement Figure 7 in Section 5.5.

A. Evaluation using Ranking Block (Binary Classifier)

In Figure 3, we showed two possible mechanisms for training a model. We can use embeddings to compute the cosine distance between two images. The results reported in the main body of paper (i.e., Table 4 in Section 5.2) are CS models built with this mechanism. Alternatively, also shown in Figure 3 (bottom-right), we can use a ranking

block to derive a binary classifier. Here we report additional experiments for this alternative mechanism.

Using ranking block is beneficial for training the CS models, and it is necessary when data is sparse. Additionally, we can also use the ranking block to conduct testing and inference. As shown in Table 7, The performance of the ranking blocks on their corresponding CS clusters is better than using the embeddings (cf. Table 3). The ranking blocks fine-tuned from ResNet18 (pretrained on Place365) consistently perform the best on all of the data clusters (highlighted). More specifically, the ranking blocks achieved 89.7% on average, which is 5.5% higher than using distances between embeddings as shown in Table 3. Due to the better performance on the CS clusters than using embeddings, it is worthy studying the performance of the ranking blocks.

To evaluate the performance of the ranking block (binary classifier O) and the trained backbone model (f), we use three metrics: 1) accuracy, 2) symmetry accuracy (swapping the two candidates and flipping the label), and 3) symmetry score defined as:

$$\begin{aligned} &|O(f(R), f(A), f(B)) \times M(R, A, B) \\ &+ O(f(R), f(B), f(A)) \times M(R, B, A)| \end{aligned}$$

where $O(f(R), f(A), f(B))$ is the confidence score (output after softmax function) of the ranking block given a triples (Reference, Candidate A, Candidate B), and $f(x)$ represents the embedding of an input image x . We denote the final binary prediction of the whole model M (including the backbone f and the ranking block O) as $M(R, A, B)$. Note that, if the binary classifier is able to predict both (R, A, B) and (R, B, A) correctly, then $M(R, A, B) = -M(R, B, A)$.

Ambiguous Triples: Despite of the satisfactory performance on the CS clusters, using the ranking block for inference can bring in other problems. We define a triple as ambiguous for the model M if the ranking block outputs the same prediction when we swap the two candidates, i.e., $M(R, A, B) = M(R, B, A)$. When using the binary classifier, to deal with ambiguous triples, we first check the confidence scores of the triples, i.e., if $O(f(R), f(A), f(B))$ is greater than $O(f(R), f(B), f(A))$, then we use the prediction of the former as the final prediction. If the confidence scores are the same, we can compare the distance between the embeddings obtained from the backbone f .

Symmetry Scores: We investigate whether the ranking blocks can produce consistent predictions when swapping the two candidates. We show the averaged symmetry scores of each ranking block in Table 8. We test each ranking block on the same CS cluster that it was trained on, as well as all other seven different CS clusters. And the results show that the trained ranking blocks are more symmetric when the reference image has been seen.

Table 7. Performance of different context-sensitive models (trained on the context training dataset) on the corresponding testing dataset using ranking block (binary classifier)

<i>Keywords Extraction and Linear Regression</i>									
Reference Image	#Indoor	#City	#Ocean	#Field	#Mountain	#Forest	#Flower	#Abstract	Average
ResNet18-Place365	67.4%	71.3%	72.7%	70.1%	69.5%	70.9%	55.8%	62.2%	60.2%
ResNet18-ImageNet	64.2%	68.2%	64.8%	58.3%	68.6%	61.8%	50.2%	55.9%	56.1%
ViT-ImageNet	75.3%	74.5%	60.6%	58.4%	57.9%	54.5%	52.5%	63.5%	61.9%

<i>Our Models (Ranking Blocks) - Different Pre-trained Architectures</i>									
Reference Image	#Indoor	#City	#Ocean	#Field	#Mountain	#Forest	#Flower	#Abstract	Average
VGG11-ImageNet	87.0%	86.0%	86.8%	87.7%	88.1%	89.3%	87.3%	81.2%	86.7%
VGG13-ImageNet	88.0%	83.6%	88.4%	86.6%	87.6%	89.3%	88.8%	83.8%	87.0%
VGG16-ImageNet	88.3%	84.9%	85.4%	89.3%	90.1%	86.9%	89.1%	79.8%	86.7%
ResNet50-ImageNet	60.6%	61.4%	66.7%	68.3%	62.9%	64.8%	61.1%	55.8%	62.7%
ResNet34-ImageNet	72.2%	71.0%	73.4%	68.4%	75.2%	74.8%	73.9%	63.6%	71.6%
ResNet18-ImageNet	87.7%	83.0%	89.8%	88.4%	88.3%	89.8%	87.9%	80.8%	87.0%
ResNet18-Place365	88.6%	88.4%	91.0%	91.3%	92.8%	90.1%	90.1%	85.6%	89.7%
Lora-ViT	87.1%	82.7%	83.8%	80.6%	85.3%	90.1%	85.9%	79.6%	84.4%

Table 8. Averaged Symmetric Scores of Ranking Blocks

CS Binary Classifier Testing Cluster	Indoor	City	Ocean	Field	Mountain	Forest	Flower	Abstract	Average
The same cluster	0.069	0.062	0.048	0.037	0.053	0.055	0.060	0.108	0.072
All other 7 different clusters	0.100	0.116	0.091	0.080	0.066	0.046	0.094	0.091	0.086

Table 9. Performance of Ensemble Models (Ranking Block) on Validation Set: 12k triples, and Testing Set: 10k triples.

	Best Single	Majority Vote	Ensemble(PCA)	Ensemble(MLP)
Validation Set	58.8%	57.1%	84.1%	78.7% ± 0.6%
Testing Set	58.7%	57.3%	69.5%	71.5% ± 1.0%

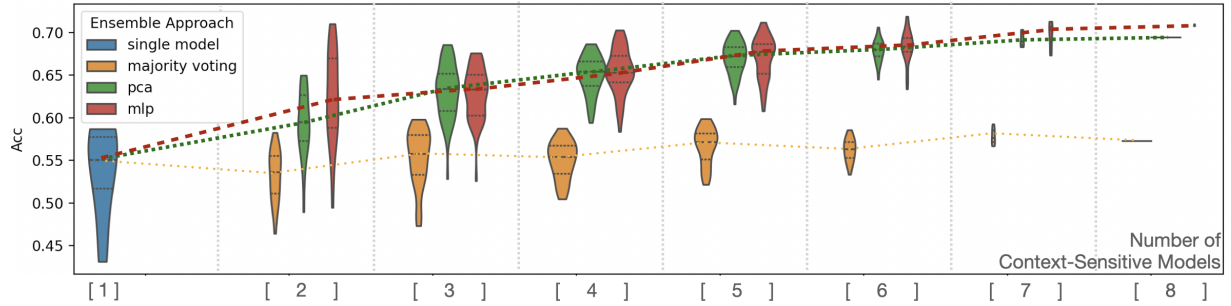


Figure 8. Y-axis: accuracy of the ensemble methods on the testing set (10k). X-axis: the number of CS models used to form the ensemble model. Experiments are run on all the combinations, e.g., when choosing two CS models, we run experiments on all of the $C_2^8 = \frac{8!}{2! \cdot 6!} = 28$ combinations. For MLP, we repeat the same experiment three times for one combination, e.g., for choosing two CS models, we run $3 \cdot C_2^8 = 84$ experiments. MLP-based approach consistently performs the best. Dashed lines inside the blobs are the quartiles of the data.

Ensemble Models: We also construct ensemble models using the binary classifiers, and test the ensembles on the randomly collected triples, i.e., our validation set (12k triples) and testing set (10k triples). As shown in Table 9, the ensemble model of ranking blocks achieved around 78%~84% on the validation set, and ~70% on the testing set. The results are significantly better than any of the single CS model (binary classifier) and majority voting. However,

the results are 10~15% worse than using embeddings as shown in Table 5 (which is expected as the ranking blocks are trained from scratch using 667 triples only). Similarly to Figure 6 in section 5.5, we also show the accuracy scores of the ensemble models increase when the number of the CS models (using binary classifiers) increases in Figure 8. Due to the worse performance on random unseen triples, in the main paper, we focused on the ensemble models con-

Table 10. Cross Validation: performance of each context sensitive models, global model and ensemble models on all of our context datasets.

<i>Performance of each context-sensitive models on each context dataset</i>									
Model \ Dataset	#Indoor	#City	#Ocean	#Field	#Mountain	#Forest	#Flower	#Abstract	Average
Model: Indoor	88.0%	85.7%	84.7%	71.0%	88.9%	79.9%	74.8%	68.8%	80.2%
Model: City	55.4%	87.5%	79.0%	70.4%	82.3%	81.7%	77.8%	69.4%	75.4%
Model: Ocean	71.9%	82.1%	89.5%	76.7%	90.4%	65.3%	70.0%	70.9%	77.1%
Model: Field	79.0%	77.6%	87.1%	90.1%	86.2%	81.4%	54.7%	70.9%	78.4%
Model: Mountain	76.0%	85.1%	85.0%	75.5%	90.7%	81.4%	82.9%	75.4%	81.5%
Model: Forest	57.8%	76.4%	75.4%	83.3%	87.7%	86.2%	86.2%	58.3%	76.4%
Model: Flower	59.9%	70.4%	76.0%	76.1%	82.6%	79.0%	86.8%	52.3%	72.9%
Model: Abstract	57.2%	77.6%	81.7%	77.3%	90.6%	84.7%	72.4%	83.8%	78.2%
Average	68.2%	80.3%	82.3%	77.6%	87.4%	80.0%	75.7%	68.7%	-
Average wo diagonal	65.3%	79.3%	81.3%	75.7%	87.0%	79.1%	74.1%	66.6%	-
<i>Performance of Our Global, and Ensemble Models</i>									
Model: Global	57.5%	76.4%	82.9%	74.6%	84.1%	74.9%	64.0%	67.3%	72.7%
Ensemble (PCA)	76.0%	86.9%	88.6%	85.1%	94.0%	84.4%	86.2%	80.5%	85.2%
Ensemble (MLP)	79.7%	85.1%	87.5%	89.5%	94.0%	86.8%	86.2%	81.2%	86.3%

Table 11. Ensemble (MLP-based) models with one missing CS model, performance on each context dataset.

Ensemble \ Cluster	#Indoor	#City	#Ocean	#Field	#Mountain	#Forest	#Flower	#Abstract	Average
No Indoor Model	76.0%	83.8%	86.8%	89.2%	93.7%	86.2%	87.1%	81.2%	85.5%
No City Model	81.7%	83.5%	87.4%	88.3%	93.4%	86.2%	87.7%	80.8%	86.1%
No Ocean Model	78.7%	85.1%	85.6%	90.7%	93.4%	87.7%	87.6%	81.3%	86.3%
No Field Model	73.6%	84.7%	86.2%	86.6%	93.7%	85.0%	87.9%	80.5%	84.8%
No Mountain Model	79.3%	84.4%	87.4%	90.1%	92.8%	86.2%	86.2%	80.5%	85.9%
No Forest Model	78.1%	86.5%	88.6%	89.8%	93.4%	85.9%	85.2%	80.8%	86.0%
No Flower Model	80.2%	85.6%	88.0%	89.5%	93.7%	85.9%	85.5%	81.7%	86.3%
No Abstract Model	80.2%	85.6%	87.4%	87.7%	93.1%	86.2%	86.5%	78.9%	85.7%
Average	78.5%	84.9%	87.2%	89.0%	93.5%	86.2%	86.7%	80.7%	-

Table 12. Performance of Ensemble Models with one context-sensitive model being left out on Testing Set (10k)

Missing Model:	Indoor	City	Ocean	Field	Mountain	Forest	Flower	Abstract	No Missing
Ensemble PCA	81.9%	82.0%	82.1%	82.4%	82.4%	82.7%	82.6%	82.9%	83.3%
Ensemble MLP	83.9%	83.8%	84.2%	84.5%	83.7%	84.1%	84.2%	83.9%	84.7%

structed using those CS models based the embedding distances, rather than these binary classifiers.

B. Cross Validation of CS Models

To investigate how the eight selected CS models perform on the other types of unseen reference images, we test each CS model M_i on all CS datasets $\{D_1, D_2, \dots, D_k\}$. As shown in Table 10, each CS model perform the best when the reference image is the same as the ones they are trained for, i.e., the accuracy scores on the diagonal are the highest for each CS cluster. Comparing Table 10 with Table 2, we can make the following observations:

1. Trained with small CS datasets, the fine-tuned CS models performed well on their corresponding datasets

(84%~91%)., suggesting some possible advantages of context-sensitive training.

2. As shown in the last column of Table 10, the fine-tuned CS models achieved 73%~81% across different CS datasets on average. Compared with existing models (Table 2), e.g., 75% for ResNet18 and 81.9% for ViT, individual CS models (with much smaller CS training datasets) achieve comparable results on different CS clusters on average.
3. Close examination shows that some CS models perform reasonably well on some other CS data clusters (e.g., the Indoor Model on #City, #Ocean, and #Mountain datasets), but not so well on other CS data clusters (e.g., the Forest Model on #Indoor and #Abstract datasets).

Table 13. Performance of meta-CS Models (ResNet18-Place365) trained on combined CS clusters, tested on each CS cluster. Nature: Ocean / Field / Mountain / Forest, Object: Flower / Abstract.

CS Cluster CS Model	#Indoor	#City	#Ocean	#Field	#Mountain	#Forest	#Flower	#Abstract	Average
City/Indoor	84.4%	82.1%	63.2%	49.3%	80.8%	73.7%	72.7%	56.2%	70.3%
Nature	78.4%	77.0%	68.9%	59.7%	86.8%	76.9%	63.1%	77.2%	73.5%
Object	60.2%	77.9%	74.3%	67.8%	76.6%	76.9%	68.2%	71.5%	71.7%

Table 14. Performance of different context-sensitive models (trained on the context training dataset) on the corresponding testing dataset.

<i>Our Context-Sensitive Models - Different Pre-trained Architectures</i>									
Reference Image	#Indoor	#City	#Ocean	#Field	#Mountain	#Forest	#Flower	#Abstract	Average
VGG11-ImageNet	86.5%	84.2%	85.9%	88.3%	86.9%	76.4%	67.2%	76.7%	81.5%
VGG13-ImageNet	85.9%	86.9%	84.5%	89.0%	87.1%	77.5%	68.3%	76.9%	82.0%
ResNet50-ImageNet	41.6%	66.8%	58.6%	74.3%	80.1%	60.0%	62.6%	49.6%	61.7%
ResNet34-ImageNet	50.3%	71.0%	60.2%	72.8%	83.9%	63.3%	62.6%	53.4%	64.7%

This suggests that (i) our CS models can be used on the data that they have not seen in some cases, and (ii) If we can predict statistically how our CS models will perform on unseen reference images via testing and analysis, we are able to produce a stronger ensemble model as we show in the main paper.

C. Ablation Study on Ensemble Models

To compare how eight CS models contribute to the ensemble model, we construct ensemble models using seven CS models with one CS model being left out. We run each ensemble model on the CS clusters. The results are shown in Table 11. For labelling each ensemble model in the table, “No X Model” denotes an ensemble that is composed of seven CS models without the X CS model. For example, “No Indoor Model” denotes that the CS model trained with #Indoor dataset was left out in the ensemble model.

When comparing each column, the ensemble without the X CS model often performs the worst on the X data cluster. For example, the ensemble “No City Model” performs the worst on the #City data cluster in comparison with other ensemble models with the “City” CS model as shown in the #City column. Occasionally, there are exceptions, e.g., the ensemble “No Indoor Model” is the second worst in the #Indoor column, and “No Flower Model” is the second worst in the #Flower column.

Nevertheless, in general, the performance difference in the table is much smaller than those in Table 10, and the average values in the last column also improves significantly. This indicates that (i) an ensemble of CS model can improve the overall performance of those component CS models, (ii) an ensemble of CS model can work reasonably well on a CS dataset that none of the component CS models saw previously. One interesting observation is that all ensemble models perform well ($\geq 93\%$) on the #Mountain data cluster,

including the ensemble “No Mountain Model”. This suggests that the knowledge of image similarity in the context of mountains might also be learned from other CS data clusters.

We also test the eight “No X models” on the 10k context-convolute testing set, and the results are shown in Table 12. For example, the cell “Ensemble PCA”-“Indoor” shows the result of applying the an ensemble model that consists of seven CS models excluding the Indoor Model and is constructed based on credibility maps (Section 3.1). We highlight the best and the worst results for each ensemble approach. The results show CS models have different impacts on different ensemble strategies, e.g., the mountain-sensitive model is considered the most important for the MLP-based ensemble whilst the PCA-based ensemble might consider the indoor-sensitive model the most important.

All of the ensemble models perform relatively satisfactory, even on the left-out clusters. Compared with results of the ensemble model using all eight CS models (the last row in Table 10), the ensemble models with seven CS models only perform slightly worse on average.

D. Meta Context-sensitive models trained on combined context datasets

In the main paper, we show that training a global model on the mixtures of all CS clusters does not improve the performance. As inspired by [1] where randomized meta-proxies are shown to be more effective, we also run experiments on meta-CS models trained on meta-CS clusters. In Table 13, we show performance of meta-CS models trained with two or three CS clusters. To be more specific, we train: 1) City/Indoor-sensitive model with the City and Indoor clusters, 2) Nature-sensitive model with the Mountain, Forest, Ocean, and Field clusters, 3) Object-sensitive model with

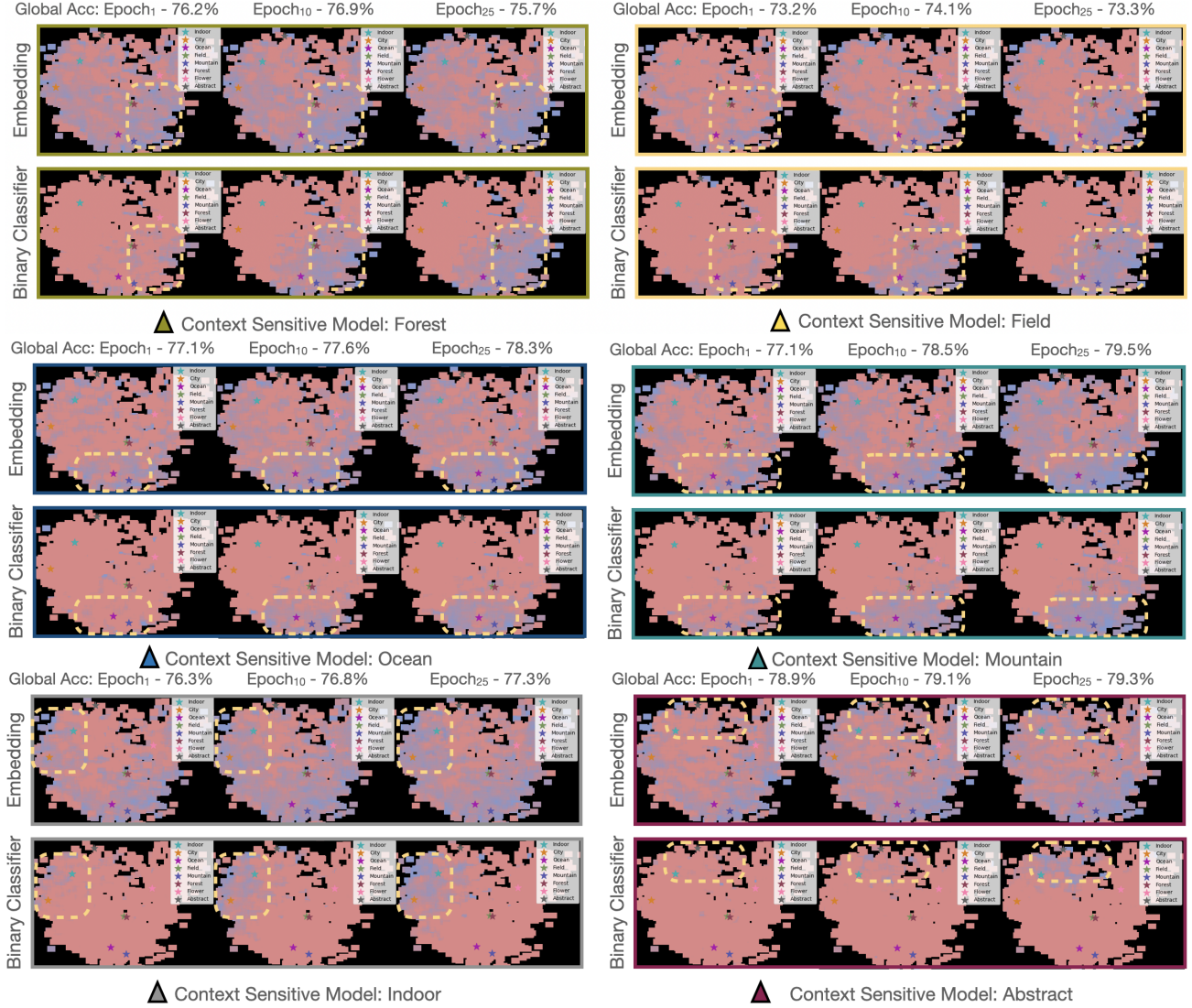


Figure 9. More visualized CS training process: all of the CS models are able to improve local performance (highlighted areas) but not global accuracy. The local improvement of abstract-sensitive model (on the right) is less noticeable because 1) there are not too many “abstract” reference images in the validation set, and 2) the “abstract” images might not be grouped together when applying dimension reduction, e.g., tSNE or PCA.

the Abstract and Flower clusters. The three meta-CS models achieved 70%~73% on average when applied to different CS clusters, which is similar to the performance of the global models (Table 6). Additionally, compared with individual CS models (as shown in Table 10), the meta-CS models do not perform well on any of the individual CS clusters. The results provides more evidence supporting the observation that training a global model on the mixtures of all CS clusters does not improve the performance. Therefore, when assembling the CS-models, we consider only the CS models, each of which is trained with only one CS cluster.

E. More Testing Results and Training Details

To complement Table 3 in Section 5.2, we also train CS models using other different architectures as shown in Table 14. The results show that training CS models using larger architectures might not be efficient, e.g., ResNet50 achieved only 61.7% on average whilst VGG11 and VGG13 achieved over 81%. Therefore, in the main paper, we report our best CS models with a smaller architectures, e.g., ResNet18, or a larger architectures trained with LORA [14]. Similarly to Figure 7 in section 5.5, we also show the CS training process for more CS models in Figure 9. All the CS models are able to acquire knowledge to improve local perfor-

mance whilst the global performance remains stable during CS training.

Training CS models: when training each CS model, we use the following setting: 1) learning rate: 10^{-4} for ViT with LoRA, and 10^{-5} for others architectures, 2) number for epochs: 25, 3) loss: cross entropy + $0.1 * \text{triplet loss}$, 4) batch size: 8, 5) optimizer: adam, 6) single image augmentation: random resized crop and horizontal flip, 7) triples augmentation: randomly swap candidate A and B, 8) normalization: (0.485, 0.456, 0.406), (0.229, 0.224, 0.225), 9) all images resized to: 224×224 . We did not carefully tune the hyper-parameters. Due to the small size of each CS cluster, we are able to train all of our CS models on one single laptop with Apple M1 Chip. The training time of each CS model varies from one day to three days (with ViT and LoRA), whilst the training time of the global models can be as long as two weeks (with ViT and LoRA). With the limited resources and limited amount of labelled data, we are able to improve the performance on the problem of context-sensitive image similarity using the proposed methodology.